A Cooperative Integration of Stereopsis and Optic Flow Computation

G. Sudhir*   Subhashis Banerjee†   K.K. Biswas†   R. Bahl‡

Abstract

A cooperative integration of stereopsis and optic flow computation is presented. Central to our approach is the modelling of the visual processes as a sequence of coupled MRF's by defining suitable inter-process interactions based on some natural constraints. The integration makes each of the individual processes better constrained and more reliable. Further, as a result of the integration, it becomes possible to accurately preserve the discontinuities in both the flow and the disparity fields along with the regions of stereo occlusion. Results on both noisy synthetic image data and real images are presented.

*D.S.P. Laboratory, Core Technology Research Center, Samsung Advanced Institute of Technology, Suwon, South Korea 440-600. Email: sudhir@dspsun.sait.samsung.co.kr

†Dept. Computer Science and Engineering, Indian Institute of Technology, New Delhi 110016, India. Email: suban@cse.iitd.ernet.in

‡Centre for Applied Research in Electronics, Indian Institute of Technology, New Delhi 110016, India. Email: rbahl@care.iitd.ernet.in

1 Introduction

In this paper we present a cooperative integration of stereo correspondence and motion computation by optic flow. The integration is achieved by modeling the visual processes as coupled Markov random fields (MRF's) [1, 2] and by defining appropriate inter-process interactions on the basis of natural constraints. As a result of the integration, it becomes possible to obtain dense disparity and flow fields at every instant of a binocular image sequence. An important outcome of the present investigation is that the cooperative integration of stereo and optic flow facilitates the detection of discontinuities in both the disparity and the flow fields, in addition to the detection of regions of occlusions in stereo.

Stereo and optic flow computations have typically been treated as separate processes [3, 4, 5, 6, 7, 8, 9, 10]. However, when treated in isolation, the analysis of each of these processes is faced with certain inherent difficulties. The intensity based stereo methods [11, 12, 13] rely heavily on window correlations of intensity values in the left and the right images of a stereo pair. Moreover, to overcome the ill-posed nature of the stereo disambiguation problem, it becomes necessary to impose a constraint of smoothness on the resulting disparity solution. While the latter constraint breaks down at the surface boundaries with depth discontinuities, window correlations give erroneous signals at regions of occlusion and depth discontinuities. The edge based stereo methods [4, 5, 14] which try to match compatible feature points in the left and the right images using smoothness constraint along figurally continuous sections are more reliable; but such methods can only provide sparse disparity maps. On the other hand, methods of computation of optic flow also require a smoothness constraint for the resulting flow field [6, 8, 9, 10, 15, 16] which breaks down at the surface boundaries. Moreover, these methods require the image intensity gradient information at regions of continuous flow. These gradient information become unreliable, for the purpose of optic flow computations, when estimated from neighboring pixels which are projections of world points belonging to different surfaces.

We propose to overcome these problems [17] by considering a cooperative integration of stereo and optic flow computations where each process helps to correct the other. We consider, at one time, two successive binocular image pairs (as shown in Fig. 1). For time instants t_0 and $t_0 + \Delta t$, we simultaneously compute the two stereo processes and the two optic flow processes between them. At a subsequent time instant $t_0 + n\Delta t$, we simultaneously compute the stereo process at $t_0 + n\Delta t$ and the two optic flow processes between $t_0 + (n-1)\Delta t$ and $t_0 + n\Delta t$ with the stereo process at $t_0 + (n-1)\Delta t$ being held constant. The integration of the four processes, considered together, is based on the following physical constraints:

C1 discontinuities in the optic flow field indicate potential discontinuities and regions of occlusion in the corresponding disparity field

C2 discontinuities in the disparity field indicate potential discontinuities in the corresponding optic flow field

C3 if a and b are corresponding points in the left and right images at the time t, and the optic flow vectors at a and b map them to points a' and b' at time $t + \Delta t$, then a' and b' should be corresponding points (see Fig. 2). Hence, for the point a, the corresponding point is constrained to lie near the point b, which can be computed from the two optic flow processes and the other stereo process. We call this the *round-about compatibility* constraint. Thus, the separate optic flow processes can track corresponding features in a stereo pair along binocular image sequences and help in the process of stereo disambiguation by significantly reducing the search space

C4 corresponding points in a stereo pair of images must have compatible optic flow vectors, apart from having compatible image features

We make the following assumptions:

1. the stereo disparities are confined along the same horizontal scan line, within fixed minimum and maximum values

2. the motion between successive time frames is small (short range motion); so that the optic flow equation (Eqn. 6) is valid at all points within the limits of discretization.

There have been several attempts to integrate optic flow information into stereo matching using one or more of the above ideas [18, 19, 20, 21]. The constraint C4 above has been used in [20, 21] and has been termed as the constraint of relative flow (or binocular difference flow). The idea of using coupled MRF's for including optic flow information into stereo matching has also been used in [21]. While most of these methods attempt only to improve stereo matching using the optic flow results, we propose a cooperative solution of stereo and optic flow where each process aids to overcome the limitations of the other. The simultaneous use of all the four constraints mentioned above, for the identification of stereo and optic flow discontinuities, as well as the detection of regions of stereo occlusion, is the major contribution of our paper.

In what follows we briefly describe our method of integration. In Sec. 2 we formulate the problem of integration by modeling the processes as coupled MRF's, and describe our algorithm which is based on the deterministic ICM method [2, 22]. In Sec. 3 we present some results on both noisy synthetic image data and real images. Finally, in Sec. 4, we conclude the paper.

2 The problem formulation

In this section we model the visual processes as coupled MRF's. The MRF formulation allows us to define appropriate interactions between the stereo and optic flow processes and outline a solution in terms of an appropriate energy function [1, 2, 23]. The optimal solution for the disparity and the flow fields is then defined in the MAP sense and estimated using the ICM algorithm [2, 22].

For a stereo pair of images, at any time instant, the disparity and the flow fields are defined over either the left or the right image (see Fig. 1). Thus, both the processes, at a particular time instant t, are defined over the same image lattice. The disparity process is described as $\{d_{ij}\}$ where d_{ij} is the disparity value at pixel location (i, j), and optic flow process is described as $\{\rho_{ij}\}$ where $\rho_{ij} = (u_{ij}, v_{ij})$ is the flow vector at pixel (i, j). The MRF property enables us to model the interactions in terms of local probabilities for a disparity d_{ij} and an optic flow vector ρ_{ij} at pixel location (i, j), given the disparity and flow information at all other locations in the image as

$$\begin{aligned} & Prob[d_{ij} | d_{kl}, \rho_{mn} \; st \; (k,l) \neq (i,j)] = \\ & \qquad Prob[d_{ij} | d_{kl}, \rho_{mn} \; st \; (k,l), (m,n) \in N(i,j)] \qquad (1) \\ & Prob[\rho_{ij} | d_{kl}, \rho_{mn} \; st \; (m,n) \neq (i,j)] = \\ & \qquad Prob[\rho_{ij} | d_{kl}, \rho_{mn} \; st \; (k,l), (m,n) \in N(i,j)] \qquad (2) \end{aligned}$$

These local probabilities can in turn be specified in terms of local energy functions $E_d(i, j)$ and $E_\rho(i, j)$ respectively [1, 2].

In what follows, we first describe the constraints for each of the individual processes and then the define inter-process interactions through the MRF model.

2.1 The constraints of stereopsis

For a choice d_{ij}, at pixel location (i, j) on an image lattice, the constraints of stereopsis are stated as follows. We define

$$compatibility(d_{ij}) = \sum_{i_N, j_N} [L(i_N, j_N) - R(i_N, j_N + d_{ij})]^2 \qquad (3)$$

where $L(.,.)$ and $R(.,.)$ are the left and right intensity images and $(i_N, j_N) \in N(i, j)$ where $N(i, j)$ is the 3×3 neighborhood of (i, j) (including itself).

The above function measures the stereo correlation around the corresponding pixels. A small value of the function indicates that the corresponding points are stereo compatible. We define the stereo compatibility constraint as

$$compatibility(d_{ij}) \leq |N(i, j)|\delta \qquad (4)$$

where $|N(i, j)|$ is the cardinality of $N(i, j)$ and δ is a pre-defined per-pixel threshold parameter.

In addition to the above constraint, the stereo solution requires a constraint of smoothness of the resulting disparity field. A smoothness measure at location (i, j) is given as

$$smooth(d_{ij}) = \sum_{i_N, j_N} [d_{ij} - d_{i_N, j_N}]^2 \tag{5}$$

The smoothness constraint requires that at all pixels (i, j) the value of the above function should be as small as possible.

We propose to treat the data compatibility constraint as a hard constraint and define the stereo solution as one of finding the smoothest disparity field such that the compatibility constraint is satisfied at all points. However, the evaluation of both the above functions poses serious problems at the regions of surface discontinuities and depth occlusions. We propose a method for overcoming these problems in Sec. 2.3 when we describe the integration.

2.2 The constraints of optic flow

The gradient based optic flow computations methods are derived from the optic flow equation [6, 8].

$$g_x(i, j)u_{ij} + g_y(i, j)v_{ij} + g_t(i, j) = 0 \tag{6}$$

where $g_x(i, j)$ and $g_y(i, j)$ are intensity gradients along the x and y image directions and $g_t(i, j)$ is the image gradient along the time direction. These gradients can be approximated from two subsequent images at instants $t_0 + k\Delta t$ and $t_0 + (k+1)\Delta t$ using finite difference schemes in the following way (see Fig. 3):

$$\begin{aligned}
g_x(i, j) &\approx [I_{i,j+1,k} - I_{i,j,k} + I_{i+1,j+1,k} - I_{i+1,j,k} + \\
&\qquad I_{i,j+1,k+1} - I_{i,j,k+1} + I_{i+1,j+1,k+1} - I_{i+1,j,k+1}]/4.0 \\
g_y(i, j) &\approx [I_{i+1,j,k} - I_{i,j,k} + I_{i+1,j+1,k} - I_{i,j+1,k} + \\
&\qquad I_{i+1,j,k+1} - I_{i,j,k+1} + I_{i+1,j+1,k+1} - I_{i,j+1,k+1}]/4.0 \\
g_t(i, j) &\approx [I_{i,j,k+1} - I_{i,j,k} + I_{i+1,j,k+1} - I_{i+1,j,k} + \\
&\qquad I_{i,j+1,k+1} - I_{i,j+1,k} + I_{i+1,j+1,k+1} - I_{i+1,j+1,k}]/4.0
\end{aligned} \tag{7}$$

where i, j are pixel coordinates and k is the time index. The optic flow constraint requires that the optic flow equation be satisfied at all points. In addition, for rigid bodies, the following requirement of smoothness of flow must also hold at all points (i, j)

$$\|\rho_{ij} - \rho_{i_N j_N}\|^2 \leq T_\rho, \quad \forall \ (i_N, j_N) \in N(i, j) \tag{8}$$

where T_ρ is a pre-defined threshold parameter. It is obvious that the flow smoothness constraint breaks down at the boundaries of surfaces moving with different velocities.. Moreover, the estimation of the image gradients also poses problems in case an image discontinuity occurs within the region of estimation. We show that these problems can indeed be overcome by defining proper inter-process interactions which we describe next.

2.3 Interaction of stereo and optic flow

We first describe the integration of optic flow information into stereopsis.

2.3.1 Integration of Optic flow into stereo

We note that according to the constraint C1 described in Sec. 1, discontinuities in the optic flow field indicate potential discontinuities and regions of occlusion in the disparity field. To formalize the concept, we define the surface discontinuity as a binary MRF, $\Delta\rho_{ij}(i_N, j_N)$, defined over the image pixels as

$$\Delta\rho_{ij}(i_N, j_N) = \begin{cases} 1 & \text{if } \|\rho_{ij} - \rho_{i_N j_N}\|^2 \geq T_\rho \\ 0 & \text{otherwise} \end{cases} \tag{9}$$

where $(i_N, j_N) \in N(i, j)$ and T_ρ is a pre-defined threshold. Using this binary MRF, we re-define the stereo compatibility constraint as

$$\Phi_{data}(d_{ij}) = \begin{cases} 1 & \text{if } \mathit{compatibility}(d_{ij}) \leq \theta\delta \\ 0 & \text{otherwise} \end{cases} \tag{10}$$

where,

$$\mathit{compatibility}(d_{ij}) = \sum_{i_N, j_N} [L(i_N, j_N) - R(i_N, j_N + d_{ij})]^2 [1 - \Delta\rho_{ij}(i_N, j_N)] \tag{11}$$

is the correlation function as defined in Eqn. 3, with the modification that neighbors which are not flow continuous with (i,j) are left out of the correlation computation, θ is the count of neighbors which are flow continuous with (i,j) and δ is the per-pixel threshold for compatibility. Thus, $\Phi_{data}(d_{ij})$ is equal to 1 if data compatibility is satisfied and is 0 otherwise. With the above modification, the stereo correlation becomes more reliable at the object boundaries. Apart from being data compatible, the corresponding points of a stereo pair must also have compatible flow vectors, as suggested by the constraint C4 in Sec. 1. For a rigorous derivation of this constraint see [20]. Here we assume a relatively simpler form of this constraint which is valid for small motions between successive frames.

$$\Phi_{flow}(d_{ij}) = \begin{cases} 1 & \text{if } |v^L_{ij} - v^R_{ij+d_{ij}}| + ||u^L_{ij}| - |u^R_{ij+d_{ij}}|| \leq T_f \\ 0 & \text{otherwise} \end{cases} \tag{12}$$

where T_f is a pre-defined threshold. Thus, corresponding points are flow compatible if the velocity components of the corresponding points in the y-direction are similar in sign and magnitude, and velocity components in the x-direction are similar only in magnitude. Note, that for the parallel imaging geometry, a movement of the object in depth (z-direction) can result in the velocity components of the corresponding points in the x-direction having opposite signs but the flow in the y-direction must remain same.

We treat both data compatibility and flow compatibility as hard constraints which cannot be violated by any disparity assignment. It may, however, be possible that at a pixel location (i,j) there does not exist a disparity label d_{ij} which simultaneously satisfies both the constraints. For such cases, we introduce a special disparity label d^*, its physical significance being that (i,j) is either a boundary point or a point which is occluded in the other image.

In addition to these two hard constraints, and the constraint of smoothness of disparity, we also impose the constraint that a disparity assignment d_{ij} at pixel (i,j) should get adequate support from the other stereo process at the next time instant and the two optic flow processes under consideration. This is the constraint C3 (round-about compatibility) described in Sec. 1 (see Fig. 2). The constraint requires that the disparity value d_{ij} at the location a (pixel (i,j)) should point to a location near point b in the right image, where b is a point computed along the round-about path through the other stereo process and the two optic flow processes. This round-about path may not exist at all, because of a d^* assignment at the second stereo pair, or, it may not be unique. The non-uniqueness may arise while reversing the disparity values for the second stereo pair (see Fig. 1), as more than one location in the right image may be mapped by the forward stereo process to a single location in the left image. Let Λ be the set of all locations in the right image at time t which have been computed along the round-about path from a location (i,j) in the left image. Note that Λ may be an empty set. We define the round-about constraint as

$$\Phi_r(d_{ij}) = \begin{cases} 1 & \text{if } \Lambda \text{ is empty, or, } \exists (k,l) \in \Lambda \; st \; \|(i, j+d_{ij}) - (k,l)\|^2 \le T_r \\ 0 & \text{otherwise} \end{cases} \tag{13}$$

where T_r is a pre-defined threshold.

On the basis of the above constraints, we define the local energy at pixel (i,j) for a stereo process as

$$E_d(i,j) = \begin{cases} (\sum_{i_N j_N} [d_{ij} - d_{i_N j_N}]^2 [1 - \Delta\rho_{ij}(i_N, j_N)] \times & \\ \Phi_{data}(d_{ij}) \Phi_{flow}(d_{ij}) \Phi_r(d_{ij})) & \\ +[1 - \Phi_{data}(d_{ij})] C_{data} + [1 - \Phi_{flow}(d_{ij})] C_{flow} & \\ +[1 - \Phi_r(d_{ij})] C_r & \text{if } d_{ij} \neq d^* \\ & \\ C_{d^*} & \text{otherwise} \end{cases} \tag{14}$$

where, C_{data}, C_{flow} and C_r are large positive numbers signifying a high local energy if any of the hard constraints are violated (making the probability of d_{ij} negligibly small), and C_{d^*} is a constant penalty for choosing d^* which is preferable if the hard constraints cannot be satisfied, or if the smoothness constraint is badly violated. Note that the flow discontinuous neighbors have been precluded from affecting the smoothness term, as it should be at object boundaries.

2.3.2 Integrating stereo information into optic flow computation

According to the constraint C2 described in Sec. 1, a discontinuity in the disparity field indicates a discontinuity in the flow field. To formalize this concept, we define a binary MRF $\Delta d_{ij}(i_N, j_N)$ over the image pixels as

$$\Delta d_{ij}(i_N, j_N) = \begin{cases} 1 & \text{if A or B or C} \\ 0 & \text{otherwise} \end{cases} \tag{15}$$

where,

A: $d_{ij} \neq d^*, d_{i_N j_N} \neq d^*$ and $(d_{ij} - d i_N j_N)^2 > T_d$, where T_d is a pre-defined threshold

B: $d_{i_N j_N} = d^*$ and a majority of the points in the 5×5 neighborhood of (i, j) have label not equal to d^*

C: $d_{ij} = d^*, d_{i_N j_N} \neq d^*$ and a majority of the points in the 5×5 neighborhood of (i, j) have label d^*

Condition A implies that (i, j) and (i_N, j_N) are not continuous in disparity, and hence, most probably belong to different surfaces. Condition B implies that pixel (i, j) has adequate support within the region from the non-d^* neighbors and the point (i_N, j_N) is either a noise point or belongs to a different region. Condition C implies that the pixel (i, j) has maximum support from the neighbors with label d^* and probably belongs to an occluded region.

The optic flow constraint at a location (i, j) is given by Eqn. 6. However, for correct computation of the flow vector at the location (i, j), it is essential that the image gradients g_x, g_y and g_t are estimated, using finite difference schemes, from pixels belonging to the same region. This can be ensured by estimating the image gradients at (i, j) from one of the four possible frontal squares (see Fig. 3) such that $\Delta d_{ij}(i_N, j_N) = 0$ for all i_N, j_N belonging to the square. If no such square exists, the the gradients can be computed from any one of the squares.

The local energy function for the optic flow process can then be defined, on the basis of the constraints imposed by the optic flow equation and the smoothness of flow in a region, as

$$E_\rho(i,j) = \sum_{i_N, j_N} [g_x(i_N, j_N)u_{ij} + g_y(i_N, j_N)v_{ij} + g_t(i_N, j_N)]^2[1 - \Delta d_{ij}(i_N, j_N)] \tag{16}$$

Thus, we have defined the local energies $E_d(i,j)$ and $E_\rho(i,j)$ for the stereo and optic flow processes based on any one image (e.g., stereo1 and flow1 of Fig. 1). These functions can be similarly defined for the other stereo and optic flow processes which we consider together (e.g., stereo2 and flow2 of Fig. 1). The total energy of the coupled MRF's is then given as the sum total of all these local energies. In the next subsection, we briefly describe our algorithm for minimizing the total energy using the deterministic ICM method.

2.4 The algorithm

Our algorithm for obtaining an optimal solution for the coupled MRF is based on the ICM algorithm suggested in [2, 22]. We describe the algorithm for the coupled processes $stereo1, flow1, stereo2$ and $flow2$ at time instants t_0 and $t_0 + \Delta t$ which we consider together. At all subsequent time instants $t_0 + (n-1)\Delta t$ and $t_0 + n\Delta t$ the algorithm is similar, except for the fact that the stereo process at time $t_0 + (n-1)\Delta t$ is held constant.

Algorithm:

Step–1 Initialize $stereo1$ and $stereo2$ by choosing d_{ij} at each pixel (i,j) such that $compatibility(d_{ij})$ (given in Eqn. 3) is minimum.

Step–2 Initialize $flow1$ and $flow2$ by minimizing $E_\rho(i,j)$ (Eqn. 16), with $\Delta d_{ij}(i_N, j_N) = 0, \;\; \forall (i_N, j_N) \in N(i,j)$, by the method of least squares.

Step–3 For the processes $stereo1$ and $stereo2$, choose a disparity value d_{ij} for each pixel (i,j) such that $E_d(i,j)$ is minimized.

Step–4 For the processes $flow1$ and $flow2$, find an optic flow vector $\rho_{ij} = (u_{ij}, v_{ij})$ for each pixel (i,j) by minimizing $E_\rho(i,j)$ by the method of least squares.

Step–5 Repeat Steps 3-4 a fixed number of times.

Remark 1: In the local minimization of $E_d(i,j)$, in Step–3 of the above algorithm, an exhaustive search need not be made over the entire range of the disparity values. The search can be confined to the neighborhoods of those points in the other image which satisfy the constraint of the round-about compatibility. This results in a significant reduction of the search space. However, if no point satisfies the constraint of round-about compatibility, an exhaustive search is required. This ensures a possible disparity assignment for (i,j) even if its corresponding point in the next time instant has a label d^* due to occlusion. Thus, if a point is occluded in one time instant, and comes out of occlusion in the next time instant, a valid disparity label for the point is possible at the second time instant.

Remark 2: Since the total energy function for the couple MRF's is obviously non-convex, the deterministic ICM algorithm described above can only yield a local minimum. This, however, poses no serious problems in practice because the individual stereo and optic flow processes are often sufficient to obtain good starting configurations.

Remark 3: Note, that in our scheme of integration, it is necessary to reverse each stereo and optic flow process. The stereo processes need to be reversed to be able to compute the round-about paths, and the reversal of the optic flow processes are necessary for the computation of flow compatibility. The reversal is achieved, for each process, by tagging the corresponding images during the forward computations.

3 Results

In this section we present our experimental results on both noisy synthetic image data and real images.

3.1 Case Study 1: Noisy synthetic image data

We present our results for two sets of experiments on noisy synthetically generated data. In both our examples, we consider, at the instant t_0, a random-dot stereogram which gives the perception of one surface floating above the other. In this stereo pair, shown in Fig. 4, the background has a disparity of 0 pixels and the foreground (a central square region) has a horizontal disparity of 10 pixels. The images are of the size 150×150.

Example 3.1 We consider the case of a small vertical motion for the central square region with the background remaining fixed. Thus, for the time instant $t_0 + \Delta t$, the stereo images are generated from the original stereo pair by introducing a one pixel vertical shift for the central square region in both the left and the right images. We also introduce 5% uniform noise, independently, in all the four images. The results obtained, after 10 iterations of the algorithm described in the previous section, are shown in Fig. 5 and Fig. 6. In Fig. 5, we show the initial and the final disparity configurations (coded in intensity) corresponding to the stereo process at time t_0. The bright points in the final disparity configuration correspond to the label d^*. In Fig. 6, we give the corresponding results for the optic flow process based on the left image at time t_0. Similar results are also obtained for the other stereo and optic flow processes based on the right image at time $t_0 + \Delta t$.

Example 3.2 In this example, in addition to a small vertical motion of the central square region as in Example 3.1, we also consider a small horizontal motion of the background region between the successive stereo pairs. The algorithm described in the previous section was run for 10 iterations. The corresponding results for stereo and optic flow processes based on the left image at time t_0 are presented in Fig. 7 and Fig. 8. The actual directions of the flows in Fig. 8 are as shown with arrows in Fig. 9. Similar results are also obtained for the other stereo and optic flow processes based on the right image at time $t_0 + \Delta t$.

It is evident, from the final stereo and optic flow results in both examples, that we obtain the disparity and motion discontinuities with high accuracy. Also, the stereo occlusion area is accurately identifiable along with the disparity discontinuities in both the examples. This is a direct consequence of our integration scheme in which the propagation of the smoothness constraints, for both the disparity and the flow fields, is inhibited across the surface boundaries.

3.2 Case Study 2: Real Image Data

We have also tested our integration scheme on some real images. We have chosen slightly textured surfaces to ensure that the stereo correlations and the optic flow can be estimated reliably. These computations become unreliable at regions of homogeneous intensities. The two sets of real images on which we have tested our integration scheme consists of approximately square surfaces moving horizontally in front of a stationary background. We have controlled the camera movement (to obtain stereo image pairs) and the movement of the front surface (to consider motion of surfaces) using micro-precision stacks so that all the assumptions that we mentioned in Sec. 1 are satisfied.

Example 3.3 We have considered an approximately square jute surface moving horizontally in front of another stationary jute surface. The two stereo image pairs at the instants t_0 and $t_0 + \Delta t$ are shown in Fig. 10. The results obtained, after 10 iterations of the algorithm described in the previous section, are shown in Fig. 11 and Fig. 12. In Fig. 11, we show the initial and the final disparity configurations (coded in intensity) corresponding to the stereo process at time $t_0 + \Delta t$. The bright points in the final disparity configuration correspond to the label d^*. In Fig. 12, we show the corresponding results for the optic flow process based on the left image at time $t_0 + \Delta t$. Similar results are also obtained for the other stereo and optic flow processes based on the right image at time t_0.

Example 3.4 In this example, we have considered an approximately square surface of a soldering iron pad moving horizontally in front of an another stationary jute surface. The two stereo image pairs at the instants t_0 and $t_0 + \Delta t$ are shown in Fig. 13. The results obtained, after 10 iterations of the algorithm described in the previous section, are shown in Fig. 14 and Fig. 15. In Fig. 14, we show the initial and the final disparity configurations (coded in intensity) corresponding to the stereo process at time $t_0 + \Delta t$. The bright points in the final disparity configuration correspond to the label d^*. In

Fig. 15, we give the corresponding results for the optic flow process based on the left image at time $t_0 + \Delta t$.

In both examples with real image data, the final results show considerable improvements over the initial assignments. The discontinuities in the stereo and the flow fields and the area of stereo occlusion are also clearly discernible. However, the results are not as good as those obtained for the synthetic images. It should be noted that, in real images, there are many regions of homogeneous intensities. In these regions, any local method of computation of stereo disparity and optic flow is unreliable. In the case of intensity-based stereo, regions of homogeneous intensities lead to ambiguous correspondences, and, in the case of optic flow computation, the linear system of optic flow equations defined over the neighbourhood of a pixel belonging to a homogeneous intensity region tend to be ill-conditioned. We have verified that, along the borders of the central moving surface, the detection of motion discontinuities by our integration scheme has failed primarily at the homogeneous intensity regions.

In order to extend the proposed model of integration to overcome the above mentioned problems with real images, we need to impose an additional constraint that discontinuities, if any, can occur only at edge points. Thus, an edge point should be labelled, iteratively, as one of the following types: discontinuous with one neighbouring region, discontinuous with the other neighbouring region or a surface marking. Further, such an edge label should get adequate support from the labels at the neighbouring edge points. The optic flow computation also needs to be modified so that the constraint of smoothness of flow propagates along continuous regions. This is essential for dealing with regions of near homogeneous intensity so that the optic flow information near the region boundaries (where it can be computed accurately) can affect the optic flow computation in the interior ("filling in" as referred to by Horn and Schunck [6]).

The above modifications are straightforward extensions of our stereo-motion integration scheme and we are carrying out some experiments on real images with these modifications.

4 Conclusion

We have presented a scheme for the integration of optic flow computation and stereopsis based on a Markov Random Field (MRF) formulation. Central to our approach is the simultaneous use of the four constraints mentioned in Sec. 1. While the constraints C1 and C2 help in

1. inhibiting the propagation of the smoothness constraints across boundaries of different surfaces (Equation 14 and Equation 16), and in

2. restricting the neighbourhood for the computation of stereo compatibility to continuous regions,

the constraints C3 and C4 help in the process of stereo disambiguation by significantly reducing the search space. The integration makes the visual processes tightly constrained and reduces the possibility of an error. Further, it becomes possible to detect stereo occlusions and sharp object boundaries (discontinuities) in both the disparity and the flow fields. We have presented some results, both on noisy synthetic images and real images, to illustrate the proposed method. We believe that such cooperative integration is essential for the effective computation of low-level vision modules [24].

References

[1] S. Geman and D. Geman. Stochastic Relaxation, Gibbs Distributions, and Bayesian Restoration of Images. *IEEE Trans. on Pattern Anal. and Machine Intell.*, 6:721–741, 1984.

[2] R.C. Dubes and A.K. Jain. Random Field Models in Image Analysis. *Journal of Applied Statistics*, 16:131–164, 1989.

[3] D. Marr and T. Poggio. Cooperative Computation of Stereo Disparity. *Science*, 194:283–287, 1976.

[4] W.E.L. Grimson. Computational Experiments with a Feature Based Stereo Algorithm. *IEEE Trans. on Pattern Anal. and Machine Intell.*, 7:17–34, 1985.

[5] J.E.W. Mayhew and J.P. Frisby. Psychophysical and Computational Studies Toward a Theory of Human Stereopsis. *Artificial Intelligence*, 17:349–385, 1981.

[6] B.K.P. Horn and B.G. Schunck. Determining Optical Flow. *Artificial Intelligence*, 17:185–203, 1981.

[7] D. Marr and T. Poggio. A Theory of Human Stereo Vision. *Proc. R. Soc. London Ser. B*, 204:301–328, 1979.

[8] B.K.P. Horn and B.G. Schunck. Determining Optical Flow: A Retrospective. *Artificial Intelligence*, 59:81–87, 1993.

[9] P. Nesi. Variational Approach to Optical Flow Estimation Managing Discontinuities. *Image, Vision and Computing*, 11:419–439, 1993.

[10] D. Ben-Tzvi, A. Del Bimbo, and P. Nesi. Optical Flow from Constraint Lines Parameterization. *Pattern Recognition*, 26:1549–1561, 1993.

[11] S.T. Barnard and W.B. Thompson. Disparity Analysis of Images. *IEEE Trans. on Pattern Anal. and Machine Intell.*, 2:333–340, 1980.

[12] R. Nevatia. Depth Measurement by Motion Stereo. *Computer Graphics and Image Processing*, 5:203–214, 1976.

[13] D. DeVleechauwer. An Intensity-Based, Coarse-to-Fine Approach to Reliably Measure Binocular Disparity. *CVGIP: Image Understanding*, 57:204–218, 1993.

[14] S.B. Pollard, E.W. Mayhew, and Frisby J.P. PMF: A Stereo Correspondence Algorithm Using a Disparity Gradient Limit. *Perception*, 14:449–470, 1985.

[15] S.H. Hwang and S.U. Lee. A Hierarchical Optical Flow Estimation Algorithm Based on the Interlevel Motion Smoothness Constraint. *Pattern Recognition*, 26:939–952, 1993.

[16] C. Schnorr. On Functionals with Greyvalue-Controlled Smoothness Terms for Determining Optical Flow. *IEEE Trans. on Pattern Anal. and Machine Intell.*, 15:1074–1079, 1993.

[17] G. Sudhir, S. Banerjee, R. Bahl, and K.K. Biswas. A Cooperative Integration of Stereopsis and Optic Flow Computation. In *Proc. of the International Conferences on Pattern Recognition (Computer Vision and Image Processing)*, 1994.

[18] G.F. Poggio and T. Poggio. The Analysis of Stereopsis. *Annual Rev. Neurosci.*, 7:379–412, 1984.

[19] W. Richards. Structure from Stereo and Motion. *J. of Opt. Soc. of Am. Series A*, 2:343–349, 1985.

[20] A.M. Waxman and J.H. Duncan. Binocular Image Flows: Steps Towards Stereo-Motion Fusion. *IEEE Trans. on Pattern Anal. and Machine Intell.*, 8:715–729, 1986.

[21] N.M. Nasrabadi, S.P. Clifford, and Y. Liu. Integration of Stereo Vision and Optical Flow by Using an Energy-Minimization Approach. *J. of Opt. Soc. of Am. Series A*, 6:900–907, 1989.

[22] J. Besag. On the Statistical Analysis of Dirty Pictures. *Journal of the Royal Statistical Society Ser. B*, 48:259–302, 1986.

[23] F. Heitz and P. Bouthemy. Multimodal Estimation of Discontinuous Optical Flow using Markov Random Fields. *IEEE Trans. on Pattern Anal. and Machine Intell.*, 15:1217–1232, 1993.

[24] J.J. Clark and A.L. Yuille. *Data Fusion for Sensory Information Processing Systems.* Kluwer Academic Publishers, 1990.

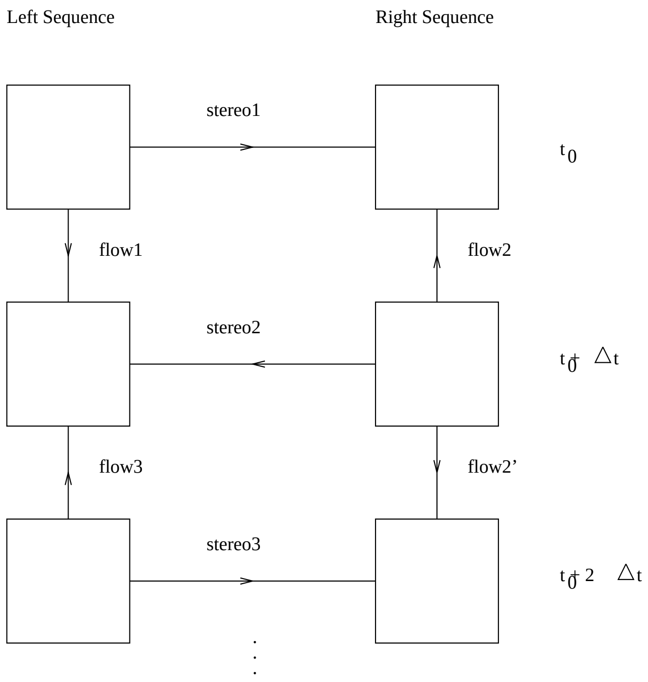

Figure 1: The scheme of integration

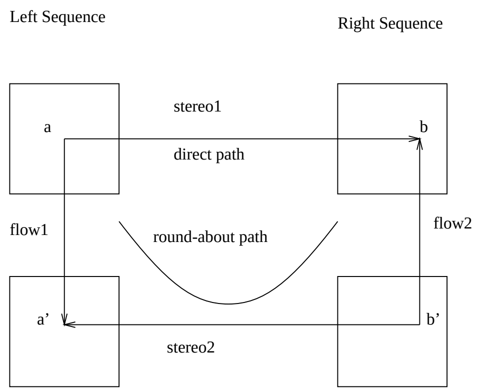

Figure 2: The constraint of round-about compatibility

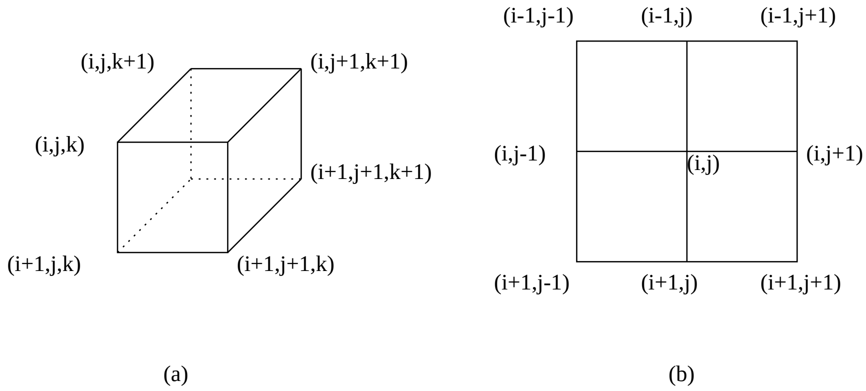

Figure 3: (a) The computation of the image gradients from two successive time frames (indexed by k) (b) At the pixel location (i, j) the image gradients can be computed from a cube (as in (a)) corresponding to any of the four frontal squares at time instant k

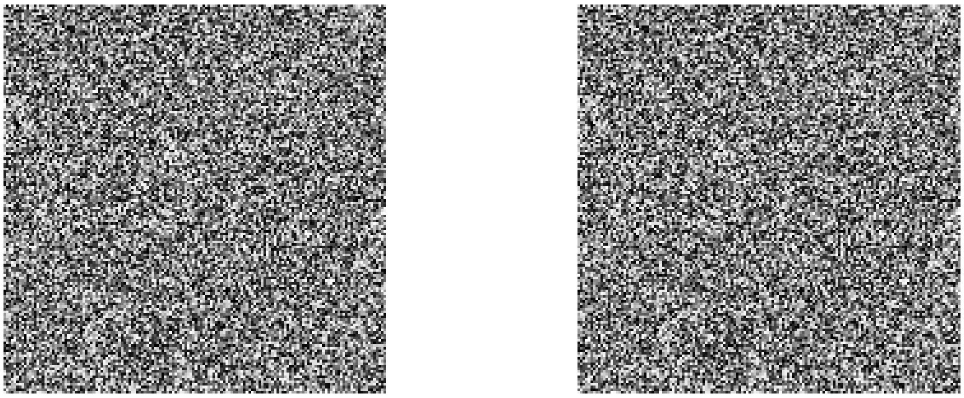

Figure 4: The random-dot stereo pair at instant t_0

Figure 5: The initial and the final disparity configuration for Example 3.1

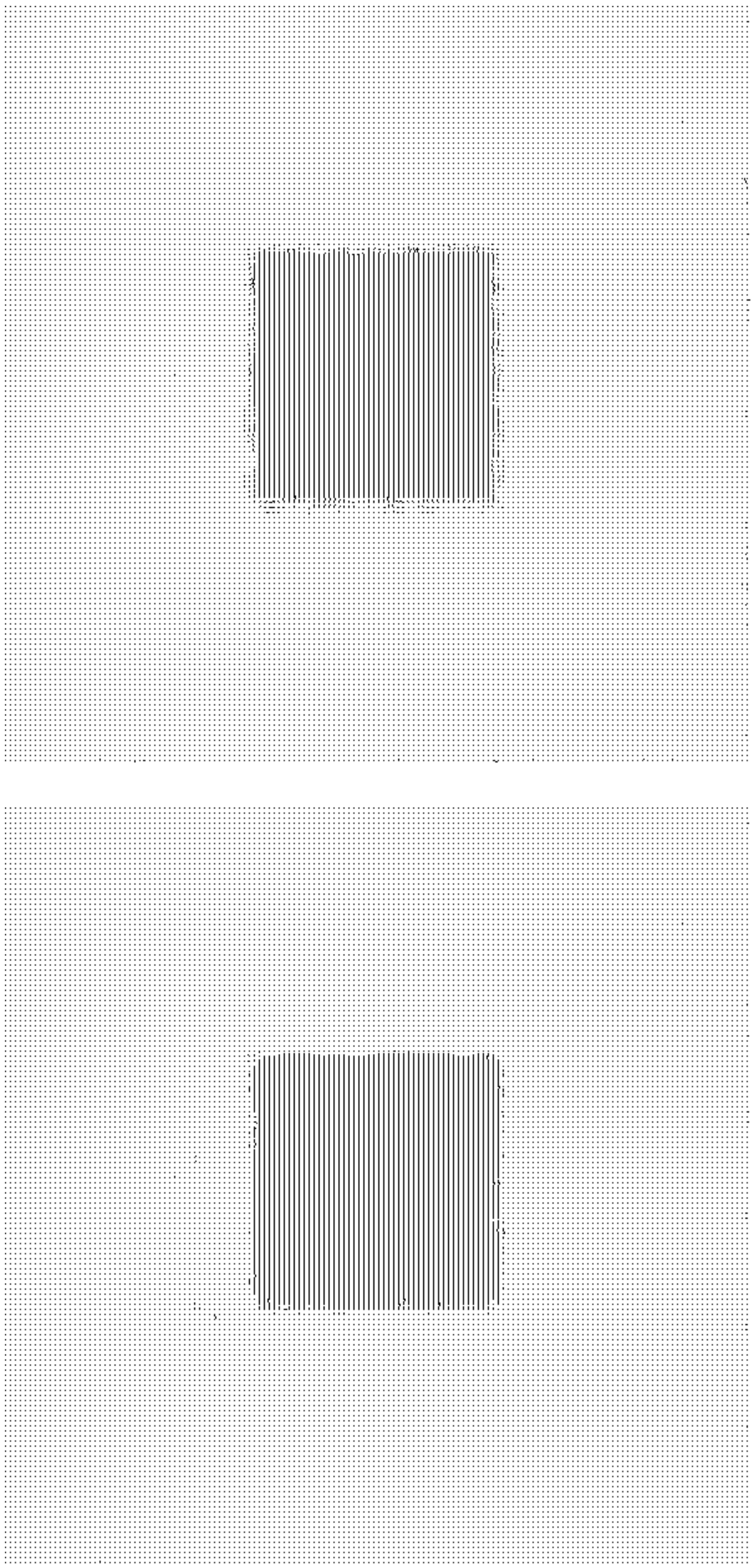

Figure 6: The initial (top) and the final (bottom) flow fields for Example 3.1

Figure 7: The initial and the final disparity configuration for Example 3.2

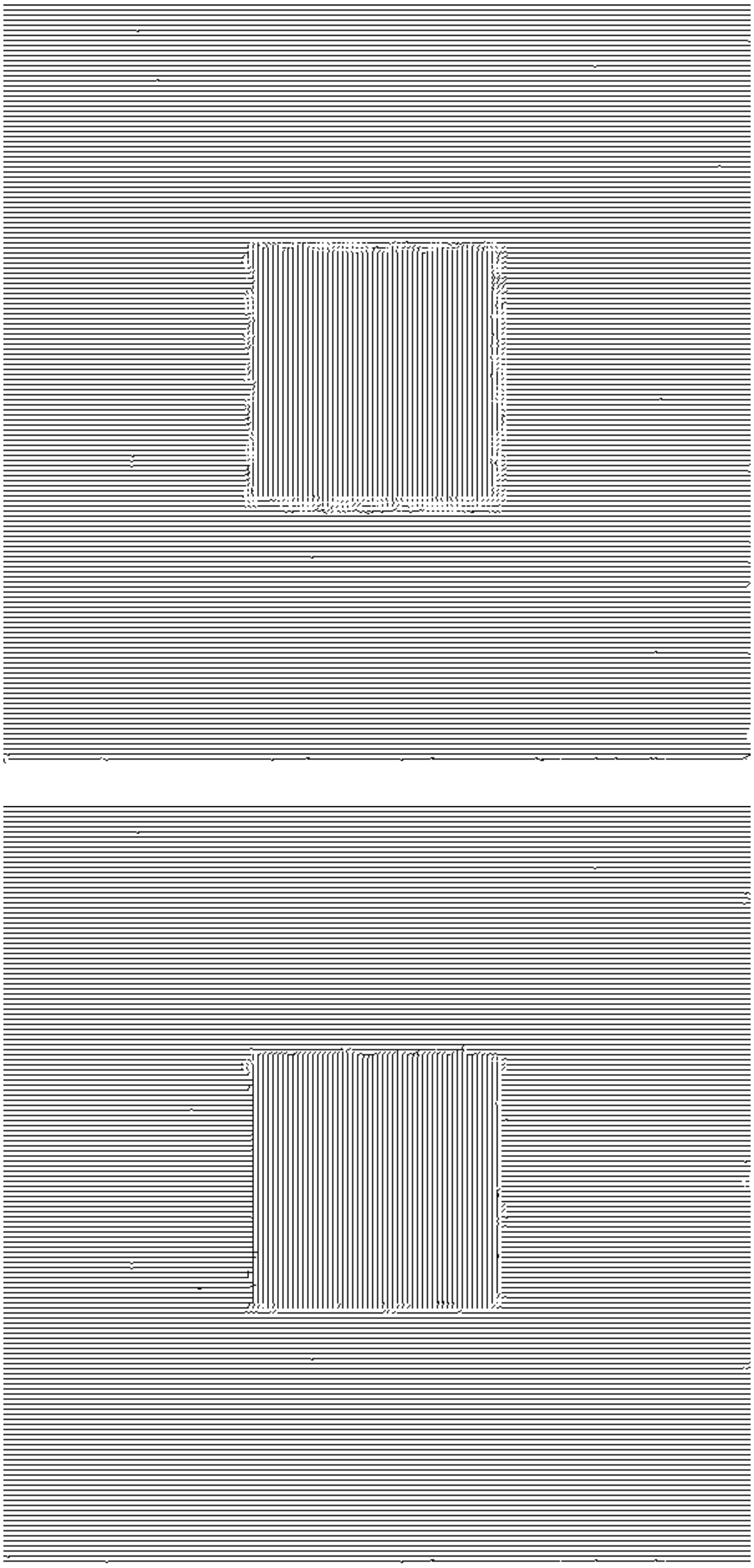

Figure 8: The initial (top) and the final (bottom) flow fields for Example 3.2

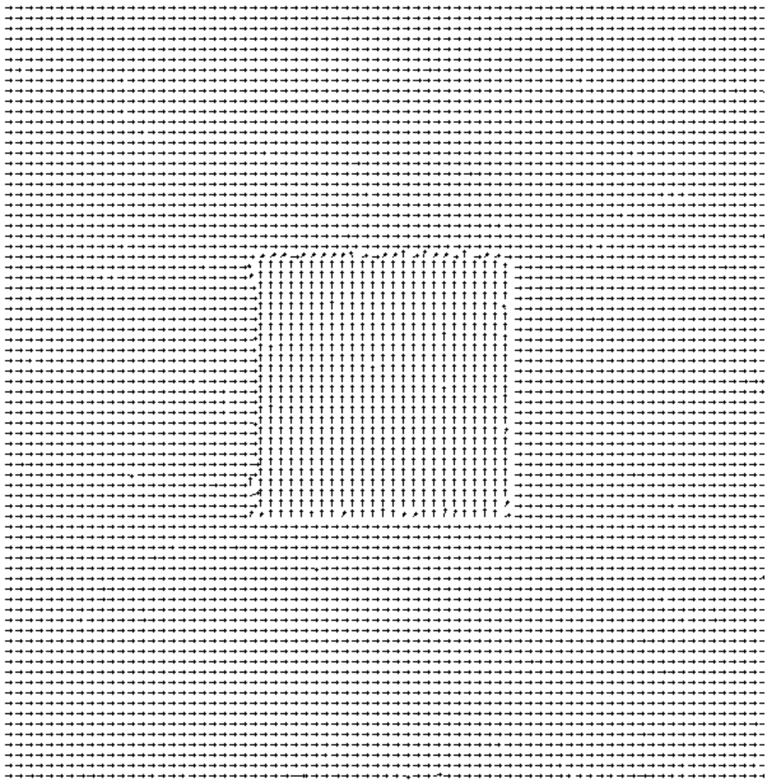

Figure 9: The final (sparse) flow field for Example 3.2 showing directions of flow

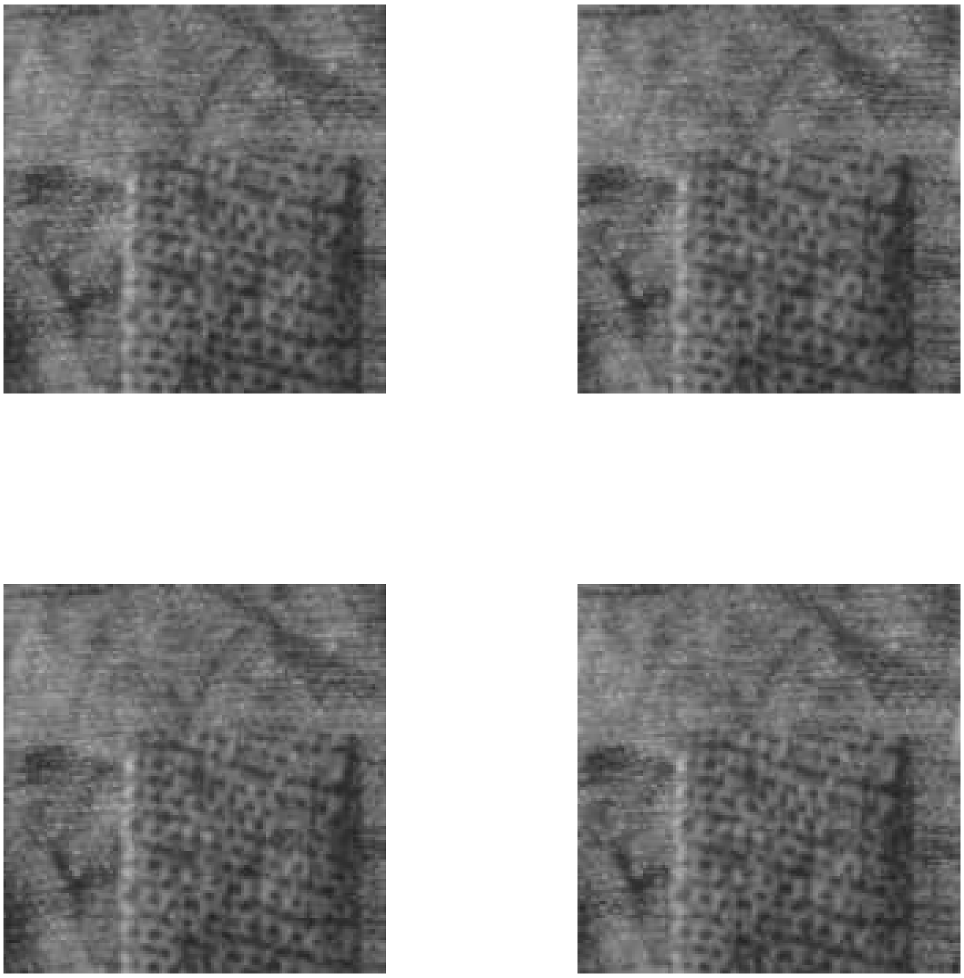

Figure 10: The two stereo pairs at instants t_0 (bottom ones) and $t_0 + \Delta t$ (top ones) for the case of an approximately square jute surface moving horizontally in front of another stationary jute surface in background (Example 3.3)

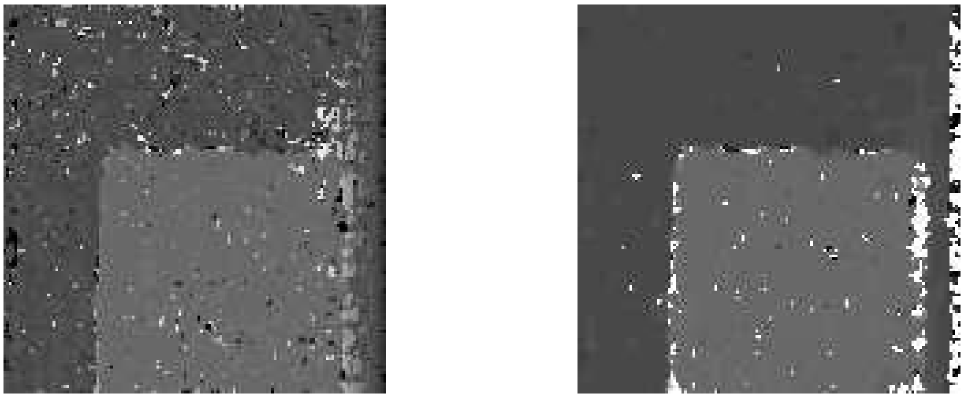

Figure 11: The initial and the final disparity configuration for Example 3.3

Figure 12: The initial (top) and the final (bottom) flow fields for Example 3.3

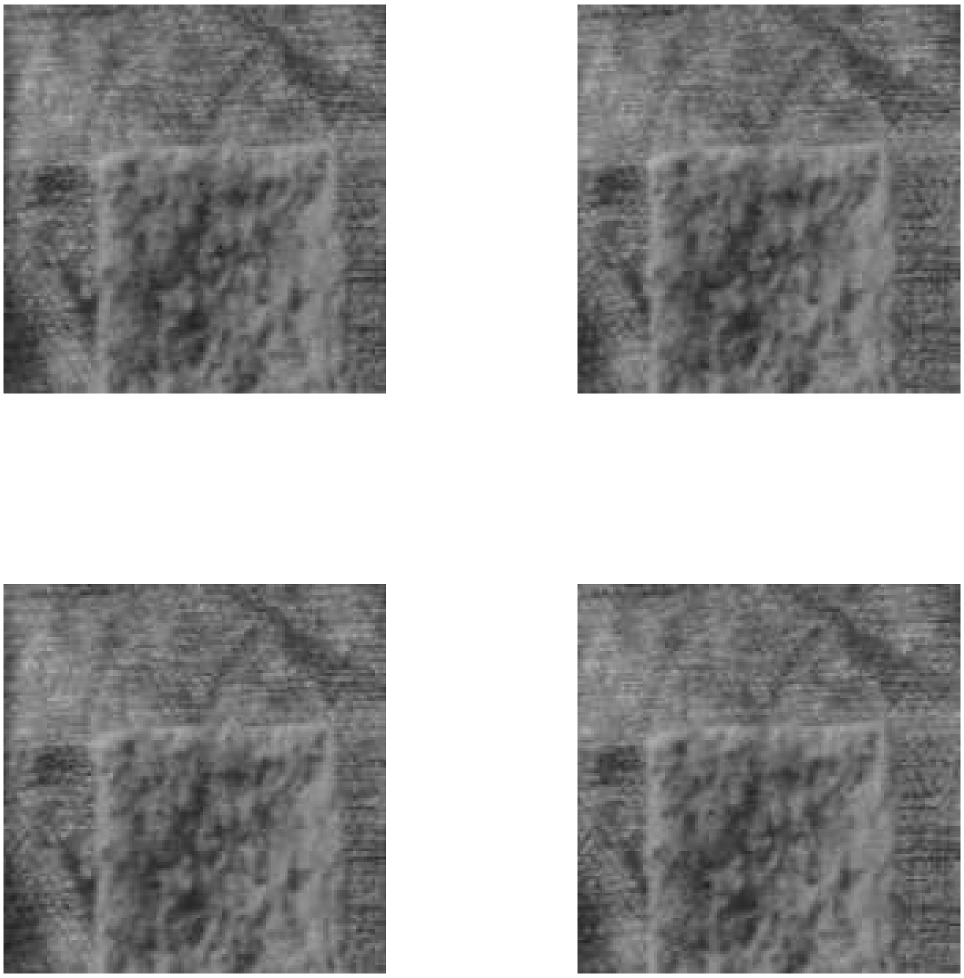

Figure 13: The two stereo pairs at instants t_0 (bottom ones) and $t_0 + \Delta t$ (top ones) for the case of an approximately square surface of a soldering iron pad moving horizontally in front of another stationary jute surface in background (Example 3.4)

List of Figures

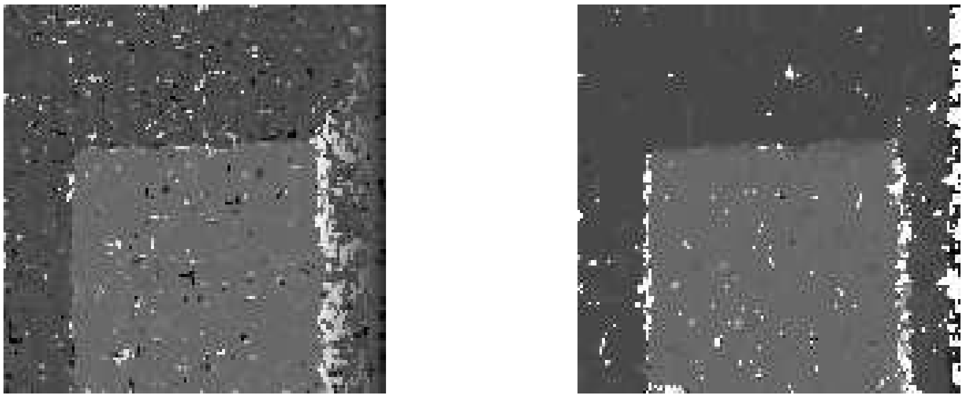

Figure 14: The initial and the final disparity configuration for Example 3.4

Figure 15: The initial (top) and the final (bottom) flow fields for Example 3.4